Optical Phonon Lineshapes and Transport in Metallic Carbon Nanotubes under High Bias Voltage

Jürgen Dietel

Institut für Theoretische Physik, Freie Universität Berlin, Arnimallee 14, D-14195 Berlin, Germany

Hagen Kleinert

Institut für Theoretische Physik, Freie Universität Berlin, Arnimallee 14, D-14195 Berlin, Germany and
ICRANeT, Piazzale della Repubblica 1, 10 -65122, Pescara, Italy
(Dated: Received December 8, 2010)

We calculate the current-voltage characteristic of metallic nanotubes lying on a substrate at high bias voltage showing that a bottleneck exists for short nanotubes in contrast to large ones. We attribute this to a redistribution of lower-lying acoustic phonons caused by phonon-phonon scattering with hot optical phonons. The current-voltage characteristic and the electron and phonon distribution functions are derived analytically, and serve to obtain in a self-contained way the frequency shift and line broadening of the zone-center optical phonons due to the electron-phonon coupling at high bias. We obtain a positive offset on the zero bias shift and no broadening of the optical phonon mode at very high voltages, in agreement with recent experiments.

I. INTRODUCTION

Carbon nanotubes are one of the strongest and stiffest materials which can sustain very high currents before breaking. This electric property makes metallic nanotubes an interesting alternative to nanometer-sized metallic wires. Since nanotubes can behave like semiconductors, their possible use in logic electronic circuits are promising. This has recently led to a number of experiments evaluating their current vs voltage characteristic at high bias voltage [1–9], with related theoretical work in Ref. 10–15.

At low voltage, the current-voltage characteristic is mainly influenced by acoustic phonons and by impurity scattering. At higher voltage, optical phonons become important. For metallic nanotubes on a substrate, the current vs voltage curve is increasing, in contrast to suspended nanotubes where the characteristic shows a negative differential conductivity at high bias [5].

We shall review in Sect. II the current-voltage characteristic of metallic nanotubes lying on a substrate. Following Refs. 11, 12 we use a Boltzmann approach for the electrons coupled to zone-center and zone-boundary optical phonons. We take into account explicitly the dynamics of the phonons by a Boltzmann equation containing an inelastic term to describe the decay of optical phonons into underlying acoustic phonons [11, 12]. We use first the so-called single-mode relaxation time approximation for the scattering term [16]. This is characterized by a thermal phonon relaxation time τ_{op}. For the electron-phonon relaxation time τ_{ep} we use a numerically determined value [10, 17], which reproduce very well the experimentally determined lifetimes of optical phonons. This proceeding agrees with the numerical work of Refs. 11, 12 in which the current-voltage characteristic of short nanotubes with lengths smaller than 1 μm is calculated. In contrast to this, Sundqvist *et*

al. [13] have in their calculation τ_{ep}-values which are around three times smaller than the experimental values. They determine the current-voltage characteristic of nanotubes larger than 1 μm using the one-valley approximation for the electrons. This implies that the electrons are scattered only by one type of phonons, i.e. zone-center phonons, between the bands within this valley. By using the experimentally determined thermal phonon relaxation life-time of $\tau_{\mathrm{op}} \approx 1.1 \pm 0.2$ps [18, 19], we reach a good agreement with the experimentally determined current-voltage characteristics of large nanotubes. This is in contrast with what happens in short nanotubes, which one has to use at least a five-times larger thermal phonon relaxation time to find a reasonable agreement with experiment.

Due to the low dimensionality of a carbon nanotube system in which a fast initial decay of optical phonons is followed by a slow decay of only a small amount of secondary acoustic phonons [20], we expect a bottleneck in the relaxation path for the hot optical phonons generated by charge carrier scattering. This idea was used in Ref. 20 to explain the large discrepancy between the radial breathing mode lifetimes measured by Raman scattering experiments, and by tunneling experiments. Such a bottleneck leads of course to larger effective thermal relaxation times for the optical phonons. In Section III we shall describe this fact effectively by taking into account in the phonon Boltzmann description the secondary acoustic phonons in a simple model. By using suitable secondary phonon relaxation times, we were able to reproduce the experimentally determined current-voltage curve also for short tubes. Our result shows that for long tubes the system does not exhibit a phonon bottleneck, in contrast to short nanotubes. We explain this by the fact that at tube length smaller than 1μm, the thermal scattering lengths of many acoustic phonons reaches the systems size which then dynamically closes

relaxation paths for the optical phonons.

We find a similar effect in the interaction of phonons with the electron system under bias voltage. It was shown in Refs. 11, 12 for short nanotubes that one finds a large increase of the phonon distribution function at the boundaries of the tube. We observe an even worse situation, that we do not find any numerical solution for the Boltzmann equation when setting the optical phonon velocities to zero. In contrast to this, we see for long tubes a phonon distribution function which is peaked in the center of the nanotube, in agreement with experiments for large suspended tubes [21]. In order to understand this effect better, we solve in Section IV the system of Boltzmann equations for the charge carriers and the phonons analytically within certain approximations. We succeeded in reproducing especially well the large-voltage small-length regime of the numerical determined current-voltage curves. Our calculation shows that the reason for the increase of the temperature at the boundary of tube is again based on the fact that using the phonon relaxation path for small tubes, the electron phonon coupling part in the phonon Boltzmann equation creates effectively an additional phonon relaxation term with a negative sign. This leads to the increase of the phonon temperatures at the boundaries of small tubes.

In the analytical calculations of Section IV we determine the electron distribution function under high bias voltages. The appearance of this distribution function is of course much different from the Fermi distribution function in thermodynamical equilibrium. The knowledge of this function opens up a number of possible applications. For example, in Section V, we calculate the level broadening and frequency shift of the zone-center optical phonons mediated by the electron-phonon interaction under high bias voltage. We find a positive frequency offset on the zero bias shift for very large bias voltages, in contrast to the frequency shift mediated by the phonon-phonon scattering with phonons in thermal equilibrium. For very large nanotubes we obtain also a negative frequency offset due to the electron-phonon interaction. The electron-phonon mediated zero-bias broadening of the zone-center optical mode vanishes at high voltages. The results for very high voltages are in agreement with a recent experiment measuring the influence of the high bias on the phonon modes of carbon nanotubes lying on a substrate [6].

Summarizing, in Sect. II we discuss the results of the coupled electron-phonon Boltzmann system in the relaxation time approximation numerically. In Section III the secondary acoustic phonons in the Boltzmann equation ia taken into account. We shall carry out in Section IV an analytical calculation of the current-voltage characteristic, the electron and the phonon distribution functions. These functions are used in Section V to calculate the level broadening and frequency shift of the optical zone-center phonons mediated by the electron-phonon interaction under high bias voltage.

II. CURRENT-VOLTAGE CHARACTERISTICS OF CARBON NANOTUBES

The method we use here to calculate the current-voltage characteristic of metallic nanotubes is based on the semi-classical Boltzmann equation. Within this method quantum interference corrections to the conductivity are not taken into account [22]. It was shown just recently through numerical calculations that these corrections to the conductivity are negligible above room temperature for single-walled carbon nanotubes without structural defects due to phonon scattering decoherence mechanisms [23]. Other works using the semi-classical Boltzmann equation for electron or phonon transport not mentioned yet are found in Refs. 24, 25.

The energy levels of electrons in a nanotube consists of one-dimensional bands positioned in the graphene Brillouin zone around the $\mathbf{K}$ and $\mathbf{K}'$ points. For metallic nanotubes two energy bands corresponding to right (R) and left (L) moving electrons cross at these points. In the following, we assume here that the diameter D of the nanotube and the applied bias voltage U is so small that we can neglect electron excitations to higher bands. For example, this is valid for a nanotube with diameter $D \approx 2$nm when we apply a bias voltage of less similar to $U \lesssim 2$V. The electron distribution functions for a nanotube under bias voltage around the $\mathbf{K}$ and $\mathbf{K}'$ points are equal which we denote by $f_{L/R}(k, x, t)$. At larger voltages only the optical phonons are relevant as a source of electron-hopping between the bands. The hopping between one band at $\mathbf{K}$ and the other at the $\mathbf{K}'$-point are mediated by zone-boundary optical phonons where only Kekulé type of lattice distortions couple to the electronic system [26]. We denote in the following the corresponding phonon distribution function by $n^{\mathrm{K}}(k, x, t)$. The hopping between bands at the same $\mathbf{K}$ or $\mathbf{K}'$ points are mediated by longitudinal zone-center optical phonons with phonon distribution $n^{\Gamma}(k, x, t)$ [10]. The time evolution of the electrons are governed by the semi-classical Boltzmann-equation

$$\left(\partial_t \mp v_F \partial_x + \frac{e\mathrm{E}}{\hbar}\partial_k\right)f_{L/R} = \left[\partial_t f_{L/R}\right]_c \qquad (1)$$

where the collision term $[\partial_t f_{L/R}]_c \approx [\partial_t f_{L/R}]_e + +[\partial_t f_{L/R}]_{\mathrm{fs}} + [\partial_t f_{L/R}]_{\mathrm{bs}}$ consists of an elastic scattering term $[\partial_t f_L]_e = v_F/l_e[f_R(k) - f_L(k)]$ due to acoustic phonon scattering (in the quasi-elastic limit) and impurity scattering. l_e is the elastic scattering mean free path. We assume here $l_e = 1600\,\mathrm{nm}$ [3, 11]. The electron velocity v_F is given by $v_F = 8.4 \times 10^7\,\mathrm{cm/s}$ and e ($e > 0$) is the electronic charge.

$[\partial_t f_{L/R}]_{\mathrm{fs}}$ is a forward scattering term which should have a minor effect especially for higher applied voltages since it does not change the propagation direction. The time evolution of optical phonons is given by

$$\left[\partial_t + v_{\mathrm{op}}^\nu(k)\partial_x\right]n^\nu = \left[\partial_t n^\nu\right]_c + \left[\partial_t n^\nu\right]_{\mathrm{osc}} . \qquad (2)$$

where $\nu = \Gamma, K$ denotes zone-center or zone-boundary phonons. We use here $v_{\mathrm{op}}^\Gamma = \mathrm{sign}(k)\, 2.9 \times 10^5\,\mathrm{cm/s}$ and $v_{\mathrm{op}}^K = \mathrm{sign}(k)\, 7.2 \times 10^5\,\mathrm{cm/s}$ [11, 17]. The term $[\partial_t n^\nu]_c$ is due to phonon-electron scattering, while the term $[\partial_t n^\nu]_{\mathrm{osc}}$ represents thermal phonon relaxation. Note that the coupled electron-phonon system is not heated up by applying large voltages on the nanotube due to this term, which accounts effectively for the scattering of optical phonons into underlying (acoustical) phonons.

Scattering of phonons with electrons leads to two scattering contributions in the electronic Boltzmann equation (1) as well as in the phononic Boltzmann equation (2). When restricting on the backward scattering contributions we obtain for the electronic scattering term

$$[\partial_t f_L]_{\mathrm{bs}} = \sum_\nu \frac{1}{\tau_{\mathrm{ep}}^\nu} \times \qquad (3)$$

$$\begin{aligned}
&\Big\{ [n^\nu(k^+, x) + 1] f_R(k_R(\epsilon^+))[1 - f_L(k_L(\epsilon))] \\
&- n^\nu(k^+, x)[1 - f_R(k_R(\epsilon^+))] f_L(k_L(\epsilon)) \\
&+ n^\nu(-k^-, x) f_R(k_R(\epsilon^-))[1 - f_L(k_L(\epsilon))] \\
&- [1 + n^\nu(-k^-, x)][1 - f_R(k_R(\epsilon^-))] f_L(k_L(\epsilon)) \Big\}
\end{aligned}$$

with $k^\pm = k_R(\epsilon^\pm) - k_L(\epsilon)$ and $\epsilon^\pm = \epsilon \pm \hbar\omega^\nu$. The corresponding phononic scattering term results in

$$\begin{aligned}
[\partial_t n^\nu]_c = \sum_\nu \frac{s^\nu}{\tau_{ep}^\nu} \times \Big(&[n^\nu(k, x) + 1] \times \\
\times \big\{ f_R(k_R^+)[1 - f_L(k_L^-)] &+ f_L(-k_L^-)[1 - f_R(-k_R^+)] \big\} \\
&- n^\nu(k, x) \times \\
\times \big\{ f_L(k_L^-)[1 - f_R(k_R^+)] &+ f_R(-k_R^+)[1 - f_L(-k_L^-)] \big\} \Big),
\end{aligned} \qquad (4)$$

where $k_{R/L}^\pm = k_{R/L}(\epsilon(k/2) \pm \hbar\omega^\nu/2)$. The number s^ν is given by $s^K = 1$ for zone-boundary phonons and $s^\Gamma = 2$ for zone-center ones [11]. In order to derive these numbers one has to take into account that momentum phase space of the phonons is twice as large as the phase space of the electrons. Further one has to consider the fact that the electron jumps from the **K** to the **K′**-band are mediated by **K**-phonons but the reverse jumps by **K′**-phonons. On the other hand jumps of electrons within the same valley are mediated by the same **Γ**-phonons. Finally, we mention here that we used the boundary conditions [11]

$$f_L(k_L(\epsilon), L) = f_R(k_R(\epsilon), 0) = n_F(\epsilon), \qquad (5)$$
$$n^\nu(k > 0, 0) = n^\nu(k < 0, L) = n_B^{\mathrm{op}}. \qquad (6)$$

where $n_F(\epsilon)$ is the Fermi function for a metallic nanotube with zero gate voltage at room temperature, i.e. $n_F(\epsilon) = 1/(1 + e^{\epsilon/k_B T})$, and n_B^{op} is the Boltzmann factor for optical phonons at room temperature given by $n_B^{\mathrm{op}} \approx 0.0014$.

We use optical phonon frequencies $\hbar\omega^K = 161\,\mathrm{meV}$ and $\hbar\omega^\Gamma = 196\,\mathrm{meV}$. The electron-phonon scattering times for zone-center and zone-boundary optical phonons are given by $\tau_{\mathrm{ep}}^\Gamma = 538\,\mathrm{fs}$ and $\tau_{\mathrm{ep}}^K = 219\,\mathrm{fs}$ [10] where we assume tube diameters of around 2.0nm typical in existing current-voltage experiments in the literature.

Our method to solve (1) and (2) is based on the numerical time integration by the standard splitting method [27]. We discretize the differential equations in momentum and position space [28]. To integrate the collisionless free electron and phonon equations in some time step, we use the exact solution of the equations in the case of the electron motion. This means that the time step value are fixed by the space grid. The free phonon motion in one time-step is given by the up integration of the collisionless discrete version of (2) on the space grid.

In this section, we use a standard single-mode relaxation time approximation for the optical phonon scattering term $[\partial_t n^\nu]_{\mathrm{osc}}$ given by

$$[\partial_t n^\nu]_{\mathrm{osc}} = -\frac{1}{\tau_{\mathrm{op}}}(n^\nu - n_B^{\mathrm{op}}). \qquad (7)$$

Note that this approximation is only valid for the system lying on a substrate. For the suspended nanotube system one has to take into account explictly the heat transfer by acoustic phonons to the leads [5]. We assume in our calculation that the thermal relaxation time τ_{op} is similar for zone-center and zone-boundary optical phonons. This approximation is justified for graphene in Ref. 30 where it is shown that the relaxation times of both phonon types are almost equal for acoustic phonon temperatures a little higher than the room temperature. We do not expect a difference for carbon nanotubes. These temperatures are immediately reached at the high voltage experiments we are interested in [6, 7, 9, 21].

First we calculate the current-voltage characteristic for nanotubes of length larger than 1μm in the vicinity of $\tau_{\mathrm{op}} = 1.1$ps. This value is chosen since Song *et al.* [18] determined experimentally $\tau_{\mathrm{op}} = 1.1 \pm 0.2$ps in agreement to the experiment of Kang *et al.* in Ref. 19.

In the upper panel in Fig. 1 the current-voltage characteristic determined with help of Eqs. (1)-(7) is shown for nanotubes at bias voltage $U = EL = 1$V as a function of their length for various relaxation times τ_{op} in the vicinity of the experimentally determined relaxation time. The solid curve in the Figure is given by the experiment carried out by Sundqvist *et al.* in Ref. 8. In this experiment the nanotube length was effectively varried by changing the distance between the electrodes where the bias voltage is applied.

We get the best agreement within the experimental uncertainties for the quantity $\tau_{\mathrm{op}} = 1.1 \pm 0.2$ps at value $\tau_{\mathrm{op}} = 0.9$ps. In the lower panel in Fig. 1, we calculate the current-voltage characteristic of nanotubes for $\tau_{\mathrm{op}} = 0.9$ps as a function of the tube length for various bias voltages. Fig. 2 shows the average phonon density for a nanotube at length $L = 3000$nm, $U = 1V$ and $\tau_{\mathrm{op}} = 0.9$.

This density is determined by

$$\overline{n}^{\nu}(x) = \frac{1}{2eEL} \int\limits_{eE(x-L)}^{eEx} d\epsilon \left[n^{\nu}(2k_L(\epsilon), x) + n^{\nu}(2k_R(\epsilon), x) \right]$$

(8)

The factor two in the denominator is necessary due to the fact that we average over the right and left moving electron bands. We obtain phonon densities which are peaked in the center of the nanotubes. This behaviour is in accordance to experiments [21] for suspended nanotubes. We show also in this figure the space averaged phonon densities $\overline{n}^{\nu} = \int dx \overline{n}^{\nu}(x)/L$ as a function of the tube length for various bias voltages.

One reason for the small difference in the current-voltage characteristic between experiment and theory in the upper panel of Fig. 1 at large nanotube lengths is due to the fact that the diameter D of the tube in the experiment Ref. 8 is in fact a little larger than 2nm. Although the diameter was not measured explicitly in Ref. 8 one can estimate it by the fact that Sundqvist *et al.* measured approximately half of the differential resistivity for short distances between the electrodes in comparison to the value in Refs. [3, 4]. In these experiments the current-voltage characteristic of short nanotubes with a measured diameter $D \approx$ 2nm was recorded. By using an analytical theory for the current-voltage characteristic which will be derived in Sect. IV and further that the electron-phonon scattering time τ_{ep}^{ν} is proportional to the diameter D of the nanotube [10] we obtain that $D \approx \sqrt{2} \times$ 2nm $\approx$ 2.8nm. We show in the upper panel in Fig. 1 by the dotted curve the theoretically calculated current-voltage characteristic for a 2.8nm nanotube, i.e. τ_{ep}^{ν} is now a factor $\sqrt{2}$ larger than for the 2.0nm nanotube already used before, and $\tau_{\mathrm{op}} = 0.9$ps.

In contrast to the small undershooting of the theoretically determined current-voltage curve in comparison to the experimental curve for large lenths in Fig. 1, we obtain for small nanotube lengths an overshooting of the curve. The reason for this different behavior between large and small nanotube lengths will be discussed in the following.

Next, we determine the current-voltage characteristic of short nanotubes. In Fig. 3 we show the current-voltage characteristic for a nanotube of length $L = 300$nm as a function of the bias voltage U for various phonon relaxation times τ_{op}. The solid curve is given by the experiment [4]. We obtain the best agreement between experiment and theory for the differential conductivity $dU/dI \approx 220k\Omega$ at $\tau_{\mathrm{op}} \approx 9.1$ps. It is astonishing that this optical phonon relaxation time is much larger than the experimentally determined optical phonon relaxation time $\tau_{\mathrm{op}} = 1.1 \pm 0.2$ps. The reason for this discrepancy will be discussed in the next section. Note that we obtain in Fig. 3 in the low voltage regime a better agreement between the theoretically and experimentally determined curves by using smaller elastic scattering lengths $l_e < 1600$nm.

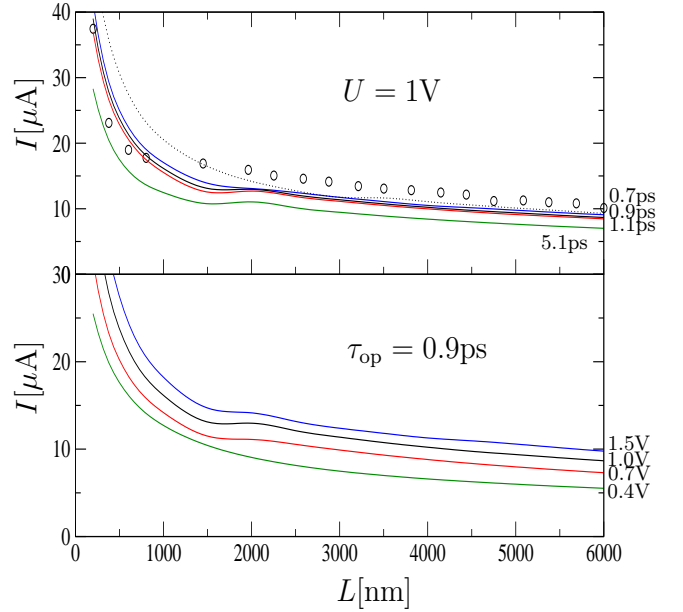FIG. 1: (Color online) Upper panel shows the current-voltage characteristic of long nanotubes with diameter $D = 2.0$nm for bias voltage $U = 1$V calculated by the help of (1)-(7) for various thermal relaxation times τ_{op} (solid curves) and $l_e = 1600$nm. The dotted curve shows the current-voltage characteristic of a $D = 2.8$nm nanotube, i.e. it uses $\sqrt{2}\tau_{\mathrm{ep}}^{\nu}$ as the electron-phonon scattering times, and $\tau_{\mathrm{op}} = 0.9$ps. The (black) circles are given by the experiment [8]. The lower panel shows the current-voltage characteristic of long nanotubes with diameter $D = 2.0$nm for various bias voltages, $\tau_{\mathrm{op}} = 0.9$ps and $l_e = 1600$nm.

III. SECOND GENERATION PHONONS

From Fig. 3 we see that a satisfactory agreement between the experimentally and numerically determined current-voltage characteristic is only reached for $\tau_{\mathrm{op}} \gg$ 1.1ps. On the other hand, recent phonon lifetime experiments on carbon nanotubes show that $\tau_{\mathrm{op}} \approx$ 1.1ps for zone-center phonons [18, 19]. These measured phonon lifetimes are governed by the decay of zone-center phonons to two lower energetic second-generation phonons where the number of these decay channels should be rather small for one-dimensional nanotube systems in contrast to higher dimensional systems like graphene or graphite [20]. The second-generation phonons are typically acoustic ones which then again scatter in two acoustic phonons with even lower energy and longer wave-length where this lifetime is much longer than of the primary optical phonons. The reason for the longer lifetime comes from the fact that the three phonon matrix element vanishes in the long-wavelength limit and further that the phase space for phonon decay is smaller for lower phonon energies due to energy conservation. The long lifetime of secondary phonons and the small amount of possible decay channels could lead to a bottle-
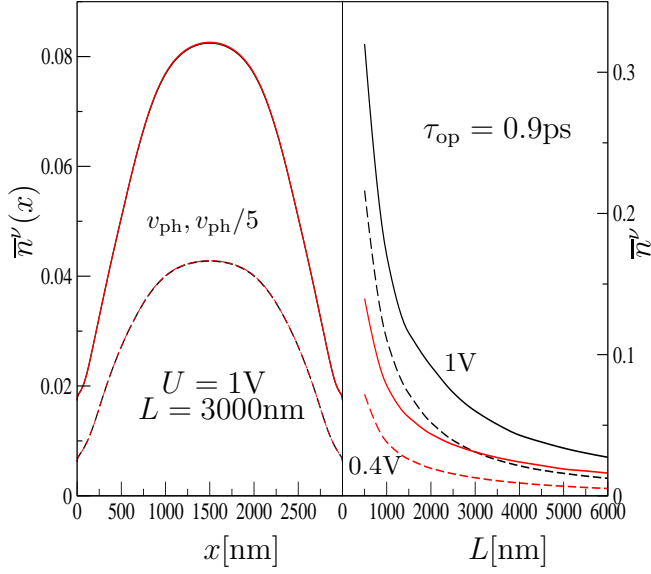
FIG. 2: (Color online) Left panel shows the phonon-density distribution functions $\overline{n}^K(x)$ (solid curves) and $\overline{n}^\Gamma(x)$ (dashed curves) defined in (8) for $U = 1$V, $\tau_{op} = 0.9$ps and $L = 3000$nm. The black curve is calculated by using the former defined $v_{op}^\Gamma = \text{sign}(k)\, 2.9 \times 10^5$ cm/s and $v_{op}^K = \text{sign}(k)\, 7.2 \times 10^5$ cm/s [11, 17]. The red curves uses $v_{op}^\Gamma/5$ and $v_{op}^K/5$ as phonon velocities. The curves lie practical on top of each other. The right panel shows position averaged phonon distribution functions $\overline{n}^K$ (solid curves) and $\overline{n}^\Gamma$ (dashed curves) for $U = 0.4$V (lower red curves) and $U = 1$V (upper black curves) for $\tau_{op} = 0.9$ps.
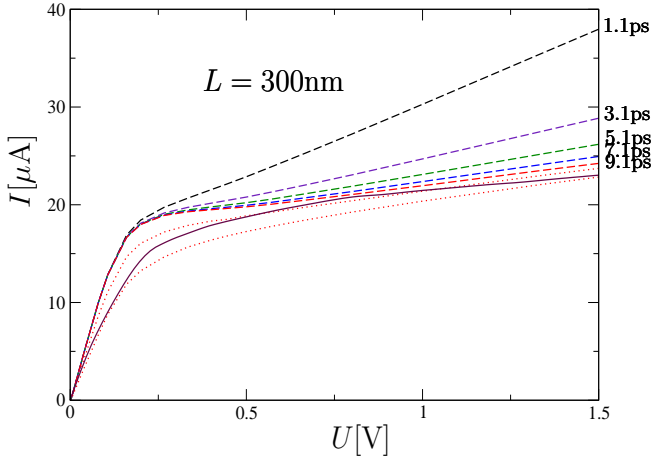

FIG. 3: (Color online) Current-voltage characteristic of a $L = 300$nm nanotube calculated by the help of (1)-(7) for various thermal relaxation times τ_{op} (dashed curves) and $l_e = 1600$nm. The (black) solid curve is given by the experiment [4]. The (red) dotted curves are calculated for $\tau_{op} = 9.1$ps, $l_e = 800$nm (upper curve) and $l_e = 400$nm (lower curve).

neck in the decay process. This means that a significant amount of secondary phonons are assembled in the decay of hot-phonons generated by charge carriers through the electron-phonon interaction. When this non-equilibrium amount of secondary phonons is similar to the number of equilibrium phonons following the Bose-Einstein distribution the single-mode relaxation time method leading to the appearance of the scattering expression (7) is no longer valid. In Ref. 20 it was argued that this fact is responsible for the considerable difference in the lifetime measurements of the radial breathing mode by using either Raman-scattering experiments or electron tunnel experiments. The decay channel can then be described by the following Boltzmann equations [31] when neglecting the phonon velocities $v_{op}^\nu \approx 0$ on the left-hand side of (2):

$$\partial_t n^\nu = \frac{1}{\tau_{op}}\left[-n^\nu(1+n_{ac})^2 + (1+n^\nu)n_{ac}^2\right] + [\partial_t n^\nu]_c \ ,$$

(9)

$$\partial_t n_{ac} = \frac{1}{p\tau_{op}}\left[n^\nu(1+n_{ac})^2 - (1+n^\nu)n_{ac}^2\right]$$
$$- \frac{1}{\tau_{ac}}(n_{ac} - n_B^{ac}) \ .$$

(10)

Here the first term in the brackets in (9) describes the scattering of the optical phonons with distribution function n^ν into two secondary phonons with distribution function n_{ac}. For simplicity we assumed that the secondary phonons follow all the same distribution function.

The second term in the brackets in (9) describes the reverse process. The second equation (10) describes the dynamics of the secondary phonons. Here p denotes the number of decay channels. For one-dimensional solids this number is generally small [20]. For simplicity we further assumed in (10) that the secondary phonons are coupled to a heat bath where the relaxation with this bath happens in time $\tau_{ac} \gg \tau_{op}$. The quantity n_B^{ac} is the Bose-factor for the secondary phonons which we assume to be half of the frequency of the optical primary phonons, leading to $n_B^{ac} \approx 0.03$ at room temperature. Note that this choice is consistent with the fact that we choose uniform secondary phonon distributions.

In the stationary case we have $\partial_t n_{ac} = 0$. Then we can solve the second equation (10) for n_{ac} and insert the result into the first equation which leads to an effective optical phonon scattering term

$$[\partial_t n^\nu]_{osc} = -\frac{1}{\tau_{op}}\left[(n^\nu - n_B^{ac})\frac{p\tau_{op}}{\tau_{ac}} - \frac{1}{2}\left(\frac{p\tau_{op}}{\tau_{ac}}\right)^2 \right.$$

(11)

$$\left. +\frac{1}{2}\frac{p\tau_{op}}{\tau_{ac}}\sqrt{\left(\frac{p\tau_{op}}{\tau_{ac}} - 2n^\nu\right)^2 + 4\left(n^\nu + \frac{p\tau_{op}}{\tau_{ac}}n_B^{ac}\right)}\right]$$
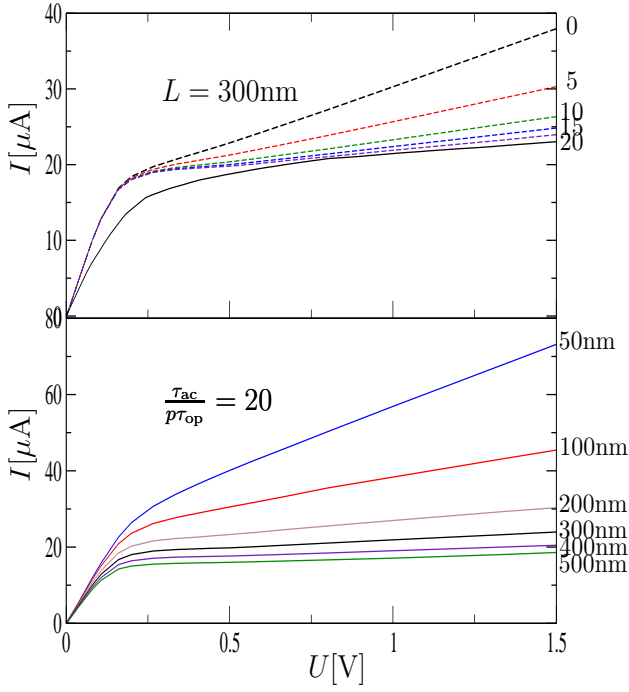
FIG. 4: (Color online) Upper panel shows the current-voltage characteristic of a $L = 300$nm nanotube calculated by the help of (1)-(4) and (11) for various parameters $\tau_{\rm ac}/p\tau_{\rm op}$ (dashed curves) and $\tau_{\rm op} = 1.1$ps, $l_e = 1600$nm. The (black) solid curve is given by the experiment [4]. The lower panel shows the current-voltage characteristic of various nanotubes with different lengths for $\tau_{\rm op} = 1.1$ps and $\tau_{\rm ac}/p\tau_{\rm op} = 20$, $l_e = 1600$nm.

FIG. 5: (Color online) Left panel shows the phonon-density distribution functions $\overline{n}^K(x)$ (solid curves) and $\overline{n}^\Gamma(x)$ (dashed curves) defined in (8) for $U = 1$V and $\tau_{\rm ac}/p\tau_{\rm op} = 20$, $\tau_{\rm op} = 1.1$ps and $L = 300$nm. The black curve is calculated by using the former defined phonon velocities $v_{\rm op}^\Gamma = \text{sign}(k)\,2.9 \times 10^5$ cm/s and $v_{\rm op}^K = \text{sign}(k)\,7.2 \times 10^5$ cm/s [11, 17]. The red curves uses $v_{\rm op}^\Gamma/5$ and $v_{\rm op}^\Gamma/5$ as phonon velocities. The right panel shows position averaged phonon distribution functions $\overline{\overline{n}}^\Gamma$ (dashed curves) and $\overline{\overline{n}}^K$ (solid curves) for $U = 1$V, $\tau_{\rm ac}/p\tau_{\rm op} = 20$ and $L = 100$nm (blue curves), 300nm (black curves) and 500nm (red curves).

with limits

$$\lim_{p\tau_{\rm op}/\tau_{\rm ac} \to \infty} [\partial_t n^\nu]_{\rm osc} \to -\frac{1}{\tau_{\rm op}} \left[n^\nu(1 + 2n_B^{\rm ac}) - (n_B^{\rm ac})^2 \right],$$
(12)

$$\lim_{p\tau_{\rm op}/\tau_{\rm ac} \to 0} [\partial_t n^\nu]_{\rm osc} \to -\frac{1}{\tau_{\rm op}} \frac{p\tau_{\rm op}}{\tau_{\rm ac}} \left[\left(1 + \sqrt{1 + \frac{1}{n^\nu}} \right) n^\nu - n_B^{\rm ac} \right].$$
(13)

As is seen from (12) in the case of no existent bottleneck, i.e. large $p\tau_{\rm op}/\tau_{\rm ac}$ and small Boltzmann factors $n_B^{\rm op}$, $n_B^{\rm ac}$ valid in our case, we obtain the standard single-mode relaxation time approximation (7) for the optical phonon scattering term.

In the following, we carry out the numerical calculation by using (1)-(4) with the optical phonon scattering term (11) substituting (7). From (11) we obtain that the optical scattering term depends via $\tau_{\rm ac}/p\tau_{\rm op}$ on the acoustic scattering length. We show in the upper panel of Fig. 4 the current voltage characteristic for various parameters $\tau_{\rm ac}/p\tau_{\rm op}$, $\tau_{\rm op} = 1.1$ps and nanotubes of length $L \approx 300$nm. This figure should be compared to Fig. 3 in the case of the single-mode relaxation time approximation which uses (7) for the optical
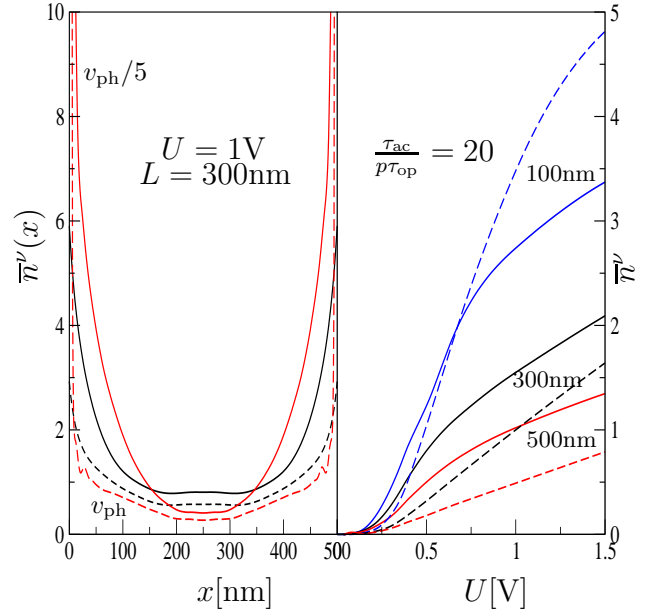
phonon scattering term. We obtain a similar behavior of the current-voltage characteristic curves in both approximations. The reason is seen from expression (13). We obtain from this expression and the fact that at room temperature $n_B^{\rm ac}, n_B^{\rm op} \ll 1$ as well as $n^\nu \gg 1$ for high bias voltages, that for small $p\tau_{\rm op}/\tau_{\rm ac}$ the effective optical phonon scattering term $[\partial_t n^\nu]_{\rm osc}$ has still the standard single mode relaxation form (7). The effective relaxation time $\tau_{\rm op}$ is then changed to $\tau_{\rm op} \to \tau_{\rm ac}/2p$ which respects the fact that the relaxation of the optical phonons are effectively relaxed on $2p$ channels of relaxation time $\tau_{\rm ac}$.

In the lower panel of Fig. 4 we show the current-voltage characteristic for various nanotube lengths by using (11) as the optical phonon scattering term with $\tau_{\rm ac}/p\tau_{\rm op} = 20$ and $\tau_{\rm op} = 1.1$ ps. Fig. 5 shows the energy-averaged phonon distribution function (8) $\overline{n}^\nu(x)$ (left panel) and the energy and position-averaged phonon distribution function $\overline{\overline{n}}^\nu$ (right panel) for various nanotube lengths. We obtain that in contrast to the case of large nanotubes in Fig. 2, the short nanotubes show an increasing phonon density at the boundary of the nanotube [11, 12]. We obtain from the left panel in Fig. 5 the even worse fact of a diverging current-voltage characteristic for phonon velocities $v_{\rm op}^\nu \to 0$. We shall understand this unusual

behaviour better in the next section where we show an analytic solution of the Boltzmann system (1)-(7).

Summarizing, by taking into account a possible bottleneck in the optical phonon relaxation path we obtain for an optical phonon relaxation time $\tau_{\mathrm{op}} = 1.1\mathrm{ps}$ for large nanotubes an effective scattering parameter $\tau_{\mathrm{ac}}/p\tau_{\mathrm{op}} = 0$ as the best fitting parameter to the experimental curves, i.e. no phonon bottleneck is seen in this case. On the other hand for small nanotubes and $\tau_{\mathrm{op}} = 1.1\mathrm{ps}$ we obtain an effective scattering parameter of $\tau_{\mathrm{ac}}/p\tau_{\mathrm{op}} = 20$. The reason for this discrepancy between large and small nanotubes lies in the fact that we have neglected the velocities of the secondary phonons in the Boltzmann equation (10). This leads in the case of the decay of zone-center optical phonons to additional terms of the form $\pm v_{\mathrm{ac}}\partial_x n_{ac}^{\pm}$ in the left hand side of (10) where $n_{ac}^{\pm}$ stands for the left and right moving phonon in a scattering pair. This means that we remove the restriction in the right hand sides of (9) and (10) that the scattering pairs have all the same distribution function. To see when the $\pm v_{\mathrm{ac}}\partial_x n_{ac}^{\pm}$ term becomes relevant in the Boltzmann equation we further have to take into account the number of decay channels p for nanotubes. In the following we restrict ourselves to the relaxation of the zone-center phonons. The argument for the zone boundary phonons works similar.

It was shown in Refs. 20, 30 that in the case of graphene the zone-center optical phonons scatter into three sorts of different pairs of phonons lying on rings in the Brioullin zone around the $\mathbf{\Gamma}$ points where scattering into the longitudinal acoustic sector is in fact the most dominant. In order to estimate from this fact the number of pairs for a nanotube with diameter of around 2nm we use in the following the zone folding approximation method. By using as an approximation that in the case of graphene the decay rings lie in the mids between the $\mathbf{\Gamma}$ and $\mathbf{K}$ point (best fulfilled for the longitudinal mode [20, 30]) we obtain as an estimate for the number of decay pairs $p \lesssim 20$ in a 2nm nanotube. In order to see no bottleneck in the relaxation process for large nanotubes we have $\tau_{\mathrm{ac}} \lesssim p\tau_{\mathrm{op}}$ meaning that $\tau_{\mathrm{ac}} \lesssim 22\mathrm{ps}$. On the other hand for a nanotube of diameter 2nm one obtains for the lowest lying phonon modes in a simple model relaxation times which are larger than around $\tau_{\mathrm{ac}} \gtrsim 20\mathrm{ps}$ [32]. This leads us to the estimate $\tau_{\mathrm{ac}} \sim 20\mathrm{ps}$ for the effective acoustic relaxation time. With $v_{\mathrm{ac}} \sim 21\mathrm{km/s}$ (we choose the maximum velocity value for acoustic phonons in graphite [33–35]) we obtain that the acoustic phonon velocity terms $\pm v_{\mathrm{ac}}\partial_x n_{ac}^{\pm} \sim \pm v_{\mathrm{ac}}n_{ac}^{\pm}/L$ in the phonon Boltzmann equation becomes relevant for $L \lesssim 420\mathrm{nm}$. This is only a very rough approximation for this length.

At this length we find that for one participant of the scattered acoustic phonon pairs this additional relaxation term is not relevant since the relaxation path is already open. For the other participant this term leads to a closing of the relaxation path which we saw in our numerics as an increase of the effective relaxation parameter $\tau_{\mathrm{ac}}/p\tau_{\mathrm{op}}$.

IV. ANALYTIC CALCULATION

Due to the similarity of the phonon frequency of zone boundary phonons ω^{K} and zone-center phonons ω^{Γ} and since the electron-phonon coupling constants $s^{\mathrm{K}}/\tau_{\mathrm{ep}}^{\mathrm{K}}$ and $s^{\Gamma}/\tau_{\mathrm{ep}}^{\Gamma}$ are similar we use in the following the simplification that the nanotube system interacts with only one sort of phonons with frequencies ω. The effective electron-phonon scattering parameter τ_{ep} in the electronic sector, the electron-phonon scattering parameter s^p/τ_{ep} in the phononic sector and phonon velocities v_{ph} are chosen in the following way

$$\hbar\omega = \hbar\left(\frac{\omega^{\mathrm{K}}}{\tau_{\mathrm{ep}}^{\mathrm{K}}} + \frac{\omega^{\Gamma}}{\tau_{\mathrm{ep}}^{\Gamma}}\right)\bigg/\left(\frac{1}{\tau_{\mathrm{ep}}^{\mathrm{K}}} + \frac{1}{\tau_{\mathrm{ep}}^{\Gamma}}\right) = 170\mathrm{meV},$$

$$\frac{1}{\tau_{\mathrm{ep}}} = \left(\frac{1}{\tau_{\mathrm{ep}}^{\mathrm{K}}} + \frac{1}{\tau_{\mathrm{op}}^{\Gamma}}\right) = \frac{1}{155\mathrm{fs}},$$

$$\frac{s^p}{\tau_{\mathrm{ep}}} = \left(\frac{s^{\mathrm{K}}}{(\tau_{\mathrm{ep}}^{\mathrm{K}})^2} + \frac{s^{\Gamma}}{(\tau_{\mathrm{op}}^{\Gamma})^2}\right)\bigg/\left(\frac{1}{\tau_{\mathrm{ep}}^{\mathrm{K}}} + \frac{1}{\tau_{\mathrm{ep}}^{\Gamma}}\right) = \frac{1}{231\mathrm{fs}},$$

$$v_{\mathrm{ph}} = \frac{v_{\mathrm{ph}}^{\mathrm{K}}}{\tau_{\mathrm{ep}}^{\mathrm{K}}} + \frac{v_{\mathrm{ph}}^{\Gamma}}{\tau_{\mathrm{ep}}^{\Gamma}}\bigg/\left(\frac{1}{\tau_{\mathrm{ep}}^{\mathrm{K}}} + \frac{1}{\tau_{\mathrm{ep}}^{\Gamma}}\right)$$

$$= \mathrm{sgn(k)}\, 5.95 \times 10^5\frac{\mathrm{cm}}{\mathrm{s}}. \tag{14}$$

In the following discussion, we use the abbreviation $l_{\mathrm{sc}}^r \equiv v_F\tau_{\mathrm{ep}}/(2\overline{n}+1)$ for the reduced effective scattering length and $l_{\mathrm{sc}} \equiv L/(1 + L/l_{\mathrm{sc}}^r)$ for the total scattering length.

Below, we solve the Boltzmann equations (1) and (2) for large voltages $eU \gg \hbar\omega$ and lengths $L \gg l_{\mathrm{sc}}^r$ analytically by the help of two approximations. In the first approximation we use in the electronic Boltzmann equation (1) positional and momentum independent phonon distribution functions $n(k,x) \approx \overline{n}$. We shall determine $\overline{n}$ then similarly to (8) where the energy average is taken over those energies where $n(k,x)$ or $f_L(k,x)$, $f_R(k,x)$ are non-zero, respectively. Thus we neglect large (infinite) energy regions where the electron and phonon distribution functions are zero since they do not contribute to the current.

In the calculation below, we find for the energy averaged phonon distribution functions

$$\overline{n}(x) = \frac{1}{2(\epsilon_u - \epsilon_d)}\int_{\epsilon_d}^{\epsilon_u} d\epsilon\, n(2k_L(\epsilon),x) + n(2k_R(\epsilon),x) \tag{15}$$

where

$$\epsilon_u = \begin{cases} eEx & \text{for } \pi\frac{eUl_{\mathrm{sc}}}{L} \gg \hbar\omega, \\ \frac{\omega L}{\pi l_{\mathrm{sc}}} & \text{for } \pi\frac{eUl_{\mathrm{sc}}}{L} \ll \hbar\omega \end{cases} \tag{16}$$

and

$$\epsilon_d = \begin{cases} eE(x - L) & \text{for } \pi\frac{eUl_{\mathrm{sc}}}{L} \gg \hbar\omega, \\ 0 & \text{for } \pi\frac{eUl_{\mathrm{sc}}}{L} \ll \hbar\omega. \end{cases} \tag{17}$$

$\overline{n}$ is then determined by the average

$$\overline{n} = \frac{1}{L}\int_0^L dx\, \overline{n}(x). \tag{18}$$

The second approximation is given by a linearization of the non-linear scattering terms in (3) which can be identified by extracting the brackets in (3). These terms are equal to the terms followed by setting in (3) n^ν equal to zero. To linearize these terms we should take care on the expansion points $\overline{f}_L$ where $f_L = \overline{f}_L + \Delta f_L$ and similar for f_R. In a first crude approximation we use in the following as the expansion point $\overline{f}_L = \overline{f}_R = 1$ which are the boundary values (5) for f_L and f_R on the non-zero momentum support of the electronic distribution function. Then we obtain

$$f_R(k_R(\epsilon + \hbar\omega^\nu))[1 - f_L(k_L(\epsilon))]$$
$$- f_L(k_L(\epsilon))[1 - f_R(k_R(\epsilon - \hbar\omega^\nu))]$$
$$\approx f_R(k_R(\epsilon - \hbar\omega^\nu)) - f_L(k_L(\epsilon)). \quad (19)$$

A. Current-voltage characteristic and electron distribution function

With the help of the approximations (18) and (19) one can solve (1) with (3) using Fourier methods. After a lengthy calculation carried out in Appendix A we obtain for the electron distribution function $f_L(x, k_L(\epsilon))$ (A5) with (A6) and (A11). The distribution function $f_R(x, k_R(\epsilon))$ is then given by $f_L(x, k_L(\epsilon))$ with the help of the substitution (A4). The current voltage characteristic is given by (A12)

$$I = 4\frac{e}{h}\left[\hbar\omega B_1\left(\frac{1 + L/l_{sc}^r}{\pi\overline{n}}\right) + \frac{eU}{(1 + L/l_{sc}^r)}\right] \quad (20)$$

where $B_1(x)$ is defined in (A13) and plotted in Fig. 6. By taking into account the regime $\overline{n} \gtrsim 1$, $v_F\tau_{ep} \approx 130$ we obtain for $L = 300$nm that $B_1 \approx 0.5$. By using $l_{sc} \approx 10.4$nm (this will be shown below by using Fig. 7) we obtain excellent agreement with the numerically determined current-voltage characteristic at high voltages shown in Fig. 3 and with experiments [3, 4] measuring $l_{sc} \approx 10 - 11$nm. Note that the first term in (20) corresponds to the y-axis value obtained by extending the high-voltage curves to this axis. For this we further note that $4(e/h)\hbar\omega \approx 26.6\mu A$.

Next, we discuss the current-voltage characteristic for large lengths, i.e. $l_{sc}/L \ll \tau_{ep}/\tau_{op}$ and low voltages $\pi eU \ll \hbar\omega L/l_{sc}$. Here, we obtain $\overline{n} \approx 1.2$ (see the discussion in Subsect. B.2) leading with Fig. 6 to $B_1 \approx 1.3$ for nanotube lengths $L \approx 3000$nm. This leads to currents which are approximately two times the current values shown in Fig. 1. Although this value is too large, the overall behavior of an approximatively length independent current for fixed bias voltage shown in the numerical calculation in Fig. 1, is also seen in the analytic calculation.

Summarizing, from (20) we obtain a different behaviour of the current voltage characteristic in the regime $\pi eU \gg \hbar\omega L/l_{sc}$ where the second term in (20) is the leading contribution to the current and the regime $\pi eU \ll$
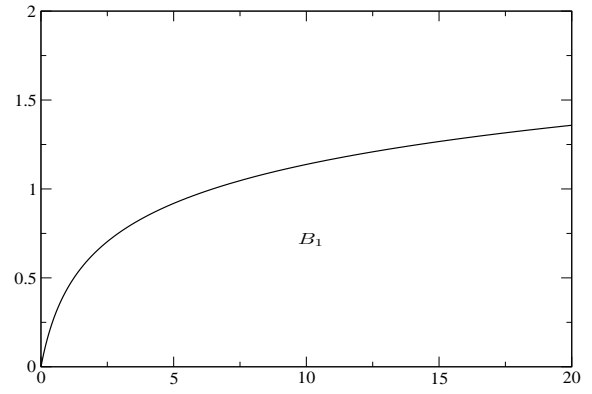

FIG. 6: (Color online) We show the function $B_1(x)$ defined in (A13).

$\hbar\omega L/l_{sc}$ where the first term is most relevant. The reason for this can be seen in (1) and (3). At low optical phonon scattering rates, i.e. $\pi eU \gg \hbar\omega L/l_{sc}$, electron scattering takes primarily place from the upper part of the filled right moving band to the empty part of left moving band. For higher scattering rates $\pi eU \ll \hbar\omega L/l_{sc}$ a large amount of electrons are also able to be scattered from the upper part of the filled right moving band to the filled part of the left moving band within many scattering processes where now Pauli blocking prohibits this scattering. This Pauli blocking is only roughly described by the linearized phonon scattering approximation (19). This is the reason that in the large length regime we obtain less agreement between our numerical and analytical results in contrast to nanotubes of smaller lengths.

B. Phonon distribution functions

Next, we determine the phonon distribution function $n(k, x)$ by solving (2) with (4) and (7). We use here in our analytical calculation for simplicity the standard relaxation time approximation (7) for the optical scattering term instead of the more complicated scattering term (11) which takes into account also the second generation phonons. As was discussed in Sect. III the differences in the current-voltage characteristic are only minor when taking the effective optical phonon relaxation times $\tau_{op} = 0.9$ps for long nanotubes and $\tau_{op} \approx 9.1$ps for short ones. We shall determine first the phonon distribution function $n(k, x)$ in the regime $\pi eU \gg \hbar\omega L/l_{sc}$.

1. Phonon distribution function for $\pi eU \gg \hbar\omega L/l_{sc}$

We obtain in App. A for $n(k, x)$ (A18), (A19) and (A20) for $k > 0$ in the different parameter regimes (A15). For $k < 0$ $n(k, x)$ is given by $n(-k, -x)$ (A14) where the K_1s are defined in (A17). From these equations we can
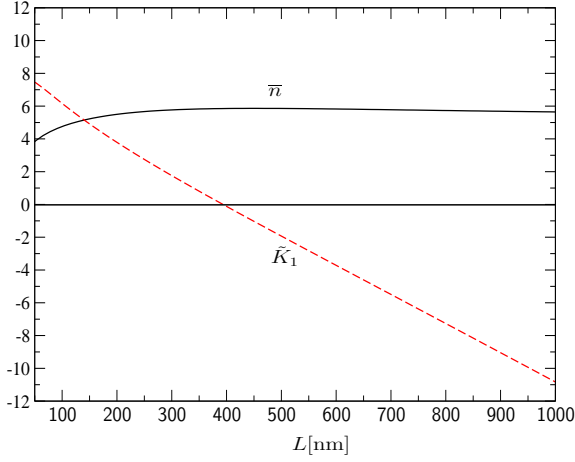
FIG. 7: (Color online) The (black) solid curve is given by the phonon distribution function $\overline{n}$ as a function of the nanotube length L calculated with the help of (A26) with (A27), (A28) and (A29). The (red) dashed curve shows $\tilde{K}_1$ (A21) as a function the nanotube length L in the parameter regime $\mathcal{R}_2$ (A17) using $\overline{n}$.

calculate the energy averaged phonon distribution function $\overline{n}(x)$. This function is given by (A22) with (A23), (A24) and (A25). From this function we obtain for the position averaged phonon distribution function $\overline{n}$ (A26) with (A27), (A28) and (A29). This function determines effectively the averaged phonon distribution function by using the definition for $\tilde{K}_1$ (A21) in the regime $\mathcal{R}_2$ (A15). We solved this equation analytically below Eq. (A30) in various nanotube length regimes. In Fig. 7 we show the numerical solutions for $\overline{n}$ and $\tilde{K}_1$ in the regime $\mathcal{R}_2$ as a function of the nanotube length L. For a nanotube of length $L = 300$nm we obtain $l_{sc} \approx 10.4$ and $\tilde{K}_1 \approx 0$. For these values we obtain (A31) for $\overline{n}(x)$ showing in fact a phonon distribution function which increases at the boundary of the nanotube. From (A25) we obtain that this behavior is even more pronounced for $\tilde{K}_1$-values larger than zero.

2. Phonon distribution function for $\pi eU \ll \hbar\omega L/l_{sc}$

In the following, we restrict ourselves to the regime where $l_{sc}/L \ll \tau_{ep}/\tau_{op}$ which is good fulfilled in the large length regime considered in Sect. II. By taking into account (A6), (A11) and (A4) we obtain that $n(k,x) \neq n_B^{ac}$ only in the regime $|\pi(\hbar v_F|k|/2\omega)L/l_{sc}| \lesssim 1$ where we take into account that $\overline{n} \lesssim 1$ as will be shown immediately below.

This leads to (A34) for $n(k,x)$ and (A35) for $\overline{n}(x)$, $\overline{n}$ in this regime. By taking into account $s^p\tau_{op}/\tau_{ep} \approx 4.76$ we obtain $\overline{n} \approx 1.2$. Note this value is much larger than the numerical determined values shown in Fig. 2.

V. THE ELECTRON-PHONON COUPLING INDUCED FREQUENCY SHIFT AND LIFETIMES OF OPTICAL PHONONS AT HIGH BIAS

By using the electron distribution functions f_L (A5) with (A6), (A11) and f_R (A4) we are now able to calculate the effect of a large bias voltage on the frequency shift and lifetimes of optical phonons. We restrict our calculation to the Raman active zone center $\mathbf{\Gamma}$ phonons. In this section, we shall carry out a similar calculation as was done in Ref. 29 for the frequency shift and lifetimes of optical phonons at zero bias voltage and temperature $T = 0$. There, the electron distribution functions f_L and f_R are Fermi-functions. The retarded phonon self-energy at zero momentum is given by

$$\Pi^{L,T}(\omega) = \sum_n \int_{-1/2}^{1/2} dt\, [\Pi^{L,T}(n,\omega) - \Pi^{L,T}(n+t,0)] \quad (21)$$

where $\Pi^{L,T}(n,\omega)$ is the self-energy contribution of the nth electron band. Its value is given by [29]

$$\Pi^{L,T}(n,\omega) = -4 \sum_{s,s'} \sum_k dt \left(\frac{\beta\gamma}{b^2}\right)^2 \frac{\hbar}{NM\omega^\Gamma} \quad (22)$$

$$\times \frac{1}{2}\left(1 \pm \frac{ss'[\kappa^2[n] - k^2]}{\kappa^2[n] + k^2}\right) \frac{f[\epsilon^s(n,k)] - f[\epsilon^{s'}(n,k)]}{\hbar\omega - \epsilon^s(n,k) + \epsilon^{s'}(n,k) + i0}$$

where the electron bands for metallic nanotubes are given by

$$\epsilon^s(n,k) = s\hbar v_F \sqrt{\kappa(n)^2 + k^2} \quad (23)$$

with $\kappa(n) = 2\pi n/L$. $s = +1$ for the energy levels in the conduction band $\epsilon > 0$ and $s = -1$ for the energy levels in the valence band $\epsilon < 0$. N is given by the number of unit cells and M is the mass of a Carbon atom. The subtraction of the last term in (21) is due to the fact that in order to calculate the frequency shift for nanotubes, we insert in the calculated expressions the known optical frequencies of graphene which then results in a double counting when we only use the first term in (21) as self-energy [29]. The valley degeneracy is here considered by a factor two in correspondence to similar expressions in Ref. 29. The upper sign corresponds to the self-energy of longitudinal phonons Π^L, the lower sign to the transversal ones Π^T

In the case of the frequency shift of the longitudinal and transversal optical $\mathbf{\Gamma}$ mode Ishikawa et al. use the zero temperature Fermi-function for $f[\epsilon^s(n,k)]$. The frequency shift $\Delta\omega$ and broadening Γ is given by [29]

$$\Delta\omega = \mathrm{Re}[\Pi(\omega^\Gamma)] \quad , \quad \Gamma = -\mathrm{Im}[\Pi(\omega^\Gamma)]. \quad (24)$$

In Ref. 29 it is then shown that this leads to a good agreement of the theoretically calculated frequency shifts

and broadenings by using (21)-(24) and the experimentally determined ones using Raman spectroscopic methods. In the following, we carry out a similar calculation for the case of the electron system under high bias voltage. For this we use for $f[\epsilon^s(n,k)]$ in (22) for the lowest energy band, i.e. $n=0$, the distribution functions f_L and f_R calculated in the last section. For the higher bands $n \neq 0$ we shall use the Fermi-function since we did not take into account higher band excitations in Sect. IV being negligible in the considered voltage regime.

$$f[\epsilon^s(n,k)] = \begin{cases} f_L(k) & \text{for } n=0 \ \& \ k \cdot s < 0 \\ f_R(k) & \text{for } n=0 \ \& \ k \cdot s > 0 \\ n_F(\epsilon^s(n,k)) & \text{for } \qquad n \neq 0 \end{cases} . \tag{25}$$

Expression (22) for the phonon self-energy corresponds to a current-current Green's function loop being the lowest order approximation for the phonon self-energy. When using dressed Green's functions by taking into account the electron-phonon interaction and also the external electric field one has to use non-equilibrium Green's function techniques in order to get the corresponding loop expression [36] for the retarded phonon self-energy. The relevant Green's functions in the loop are given by lesser $G^<$ and greater Green's functions $G^>$. We now express these Green's functions by the spectral function and use the quasi-particle approximation [36] established for deriving the Boltzmann equation. This leads to (21), (22) with (25).

It is well known that, by using the free Green's function in loops as was done by Ishikawa *et al.* [29], this approximation is conserved [37] which means that the charge-current response functions corresponding to the loop fulfill the continuity equation [37]. By using a more general dressed Green's function in the loop one needs also vertex corrections in order to fulfill the continuity equation. It is straight forward to show that the current-density correlation functions corresponding to (21), (22) with (25) which consist of dressed Green's function in loops with the additional quasi-particle approximation does indeed fulfill the continuity equation. This justifies approximation (21), (22) with (25) for the phonon self-energy at zero momentum to calculate the phonon self-energy under high bias voltage.

In the following, we use the abbreviations:

$$\tilde{\omega} = \omega \frac{\pi D}{2\pi v_F}, \tag{26}$$

$$\alpha(D) = \frac{27}{\pi}\beta^2 \left(\frac{2(\hbar v_F)}{\sqrt{3}} \right) \frac{\hbar^2}{2Ma^3} \left(\frac{1}{\hbar\omega^\Gamma} \right)^2 \frac{a}{\pi D}. \tag{27}$$

Here a is $\sqrt{3}$ times the equilibrium bond length. With the knowledge of the parameter $\tau_{\mathrm{ep}}^\Gamma = 538\mathrm{fs}$ determined by density functional methods for a nanotube of diameter 2nm [11] we are able to determine β and thus $\alpha(D)$. By using that $\tau_{\mathrm{ep}}^\Gamma$ is more generally proportional to the diameter of the nanotube [10] we obtain from (27) that

$$\alpha(D) \approx 0.1 \, a/\pi D. \tag{28}$$

With the help of (21), (22) and (25) by using the abbreviation $\Pi^L(\omega) = \Pi_{U=0}^L(\omega) + \Pi_{U>0}^L(\omega)$ we obtain

$$\Pi^T(\omega) = \alpha(D)\omega^\Gamma \left(2 - \frac{\pi^2}{9}\tilde{\omega}^2 \right), \tag{29}$$

$$\Pi_{U=0}^L(\omega) = \alpha(D)\omega^\Gamma \left(2\ln\frac{2\pi\tilde{\omega}}{e} - \frac{\pi^2}{18}\tilde{\omega}^2 - i\pi \right). \tag{30}$$

$\Pi_{U>0}^L$ is a correction factor to the zero bias self-energy $\Pi_{U=0}^L$ (30). By taking into account that $\Pi_{U=0}^T(n=0,\omega) = 0$ (22) we obtain that this factor is of similar order as the zero-bias self-energy only in the longitudinal sector for $eU \ll \hbar v_F 2/D$. Note that we restrict here ourselves also to the regime $eU \ll \hbar v_F 2/D$ as was done in the last sections by taking into account that excitations to higher bands are negligible. We obtain for the self-energy $\Pi_{U>0}^L$

$$\Pi_{U>0}^L(\omega,x) = \Pi_1^L(\omega,x) + \Pi_2^L(\omega,x) \tag{31}$$

with

$$\Pi_1^L(\omega,x) = \alpha(D)\omega^\Gamma \left\{ 2\,C(\tilde{x}) + 2\ln\left(\frac{2eU}{\hbar\omega} \right) + i\pi \right\}, \tag{32}$$

$$\Pi_2^L(\omega,x) \approx -\alpha(D)\omega^\Gamma \frac{1}{2} \left\{ (1-\tilde{x})\ln\left(\frac{|\tilde{x} + \frac{\hbar\omega}{eU\pi}\frac{L}{l_{\mathrm{sc}}}|}{\tilde{x}} \right) \right.$$
$$\left. + \tilde{x}\ln\left(\frac{|1-\tilde{x} - \frac{\hbar\omega}{eU\pi}\frac{L}{l_{\mathrm{sc}}}|}{1-\tilde{x}} \right) \right\} + \left\{ \frac{\hbar\omega}{eU\pi}\frac{L}{l_{\mathrm{sc}}} \to -\frac{\hbar\omega}{eU}\overline{n} \right\}, \tag{33}$$

where

$$C(x) \equiv x\ln(1-x) + (1-x)\ln(x). \tag{34}$$

and $\tilde{x} = x/L$. The last line in (33) means that we have to add the foregoing expressions with the substitution $(\omega/\pi)L/l_{\mathrm{sc}} \to -\omega\overline{n}$. Here Π_1^L is the self-energy part calculated by the help of $f^{t=0}$ (A6) in (22). Π_2^L is the result for $f^{t\neq0}$ (A11). In (33) we carry out for the logarithmic term in the electron distribution function (A9) the approximation that we set this term constant over the range $\pi|\epsilon - eEx_1|l_{\mathrm{sc}}/\hbar\omega L < 1$ with its value at $|\epsilon - eEx_1| = 0$ and zero elsewhere. This approximation leads to the logarithmic singularities in (33). They are softened when using the exact functions $f_L^{t\neq0}$ (A11) without approximation but this treatment has the disadvantage that we would not obtain analytical results. We should additionally mention that we neglect those imaginary terms in (32) and (33) which exist only in small regions in position space of length $\Delta x = L\hbar\omega/eU$. These correspond to regions where the ln-terms in (32) and (33) gets singular.

By taking into account the results in (30), (31), (32) and (33) we obtain the surprising result that the imaginary part of the longitudinal phonon self-energy and thus the level broadening vanishes

$$\mathrm{Im}[\Pi^L(\omega,x)] = 0 \tag{35}$$

in the high voltage-bias regime $eU \gg \hbar\omega$ in contrast to the case of no bias (30). The reason for this vanishing is seen in (22). We only obtain an imaginary part for the phonon self-energy when there is a substantial changing of the electron distribution function in the energy range $|2\epsilon| < \hbar\omega$. In the high bias regime the electron distribution function (25) becomes constant in this range which is not the case for the Fermi-function in the zero-bias system.

A. Position averaged self-energy

Finally we calculate the position averaged self-energy $\overline{\Pi}_i^L = \int dx \Pi_i^L(\omega, x)/L$. We obtain

$$\overline{\Pi}_1^L(\omega) = \alpha(D)\omega^\Gamma \left[-3 + 2\ln\left(\frac{2eU}{\hbar\omega}\right) + i\pi \right] \quad (36)$$

$$\overline{\Pi}_2^L(\omega) \approx \alpha(D)\omega^\Gamma \left[F_1\left(\frac{\hbar\omega}{\pi eU}\frac{L}{l_{\rm sc}}\right) + F_1\left(\frac{\hbar\omega}{eU}\overline{n}\right) \right] \quad (37)$$

with

$$\begin{aligned} F_1(x) &= \frac{1}{4}(x+1)^2 \left[\ln(|x|) - \ln(|1+x|) \right] - \frac{1}{4}\ln(|x|) \\ &\quad + (x \to -x) \end{aligned} \quad (38)$$

We show in Fig. 8 the function $F_1(x)$. In the regime of very high voltages $eUl_{\rm sc}/L \gg \hbar\omega/\pi$ we obtain that $\overline{\Pi}_2^L(\omega)$ is negligible in comparison to $\overline{\Pi}_1^L(\omega)$. For nanotubes of diameter 2nm we have $\tilde{\omega}_0 \approx 0.35$. Thus we obtain that $\mathrm{Re}[\Pi_{U=0}^L(\omega^\Gamma)] \approx -0.46\,\alpha(D)\omega^\Gamma$ leading to the result that $\mathrm{Re}[\Pi^L(\omega^\Gamma)] \approx \alpha(D)\omega^\Gamma[-3.48 + 2\ln(2eU/\hbar\omega^\Gamma)]$. This means that we obtain in the high voltage regime for $eU/\hbar\omega^\Gamma \gtrsim 1.8$ a positive frequency shift for the longitudinal optical phonon frequency at the Γ point. On the other hand, by taking into account that $\lim_{x\to\infty} F_1(x) = -1/2\ln(x)$ we obtain that for fixed $eU/\hbar\omega^\Gamma$ and in the large length limit $L/l_{\rm sc} \to \infty$ where $\overline{n} \lesssim 1$, that the frequency shift is negative.

B. Line-shape of Raman signal

From the considerations above it is not clear how the actual line-shape of the Stokes or anti-Stokes signal looks like in an actual Raman scattering experiment. From above we obtain first that the Raman signal corresponding to the response on transversal phonon mode excitations denoted by G^+ is not changed from the zero bias result. This is not true for the G^- Raman mode corresponding to the response on longitudinal optical phonons. In order to get a better insight into the actual Raman line-shape we assume that the incident laser light illuminates the nanotube continuously over the whole width. In typical Raman experiments the scattering of the electron system with the incident light is dominated by the resonant scattering of a valence band and conduction band of fixed index $n > 0$ (23) [38]. A further enhancement of the signal is reached when electrons from the band edges are scattered. This is due to the van Hove singularities of the density of states at this region leading not until then to the opportunity of measuring phonon and electronic properties of single nanotubes. Further let us assume in a first approximation that the phonon distribution function $n^\Gamma(x)$ (8) is homogeneous over the nanotube width which was also assumed in our analytical calculations in Sect. III. This leads us to the conclusion by taking into account that only the electron distribution function of the lowest electronic energy band $n = 0$ is changed due to the large bias voltage that we can determine at least approximately the line-shape of an actual Raman signal by the position average over the individual Raman signals.

In the following, we use the abbreviation

$$F_2(x) = \int_0^1 dy\, \delta(C(y) - x) \quad (39)$$

in order to calculate the line-shape of the Raman signal. We restrict ourselves in the following to the most important high bias regimes $\pi eUl_{\rm sc}/L \gg \hbar\omega^\Gamma$ and to the large length regime where $\pi eUl_{\rm sc}/L \ll \hbar\omega^\Gamma$, but $eU \gg \hbar\omega\overline{n}$ where we obtain simple expression for the Raman signal. By taking into account that $\mathrm{Im}[\Pi^L] = 0$ we obtain for the line-shape of Stokes and anti-Stokes signal $I_{\rm ep}$ by using (32), (33) and (39)

$$I_{\rm ep}(\omega) \propto \begin{cases} \frac{1}{2}F_2\left[\frac{\omega - \omega^\Gamma - \mathrm{Re}[\Pi_{U=0}^L(\omega^\Gamma)]}{2\alpha(D)\omega^\Gamma} - \ln\left(\frac{2eU}{\hbar\omega^\Gamma}\right)\right] \text{for } \frac{eU}{\hbar\omega^\Gamma} \gg \frac{L}{\pi l_{\rm sc}} \\ \frac{2}{5}F_2\left[\frac{\omega - \omega^\Gamma - \mathrm{Re}[\Pi_{U=0}^L(\omega^\Gamma)]}{(5/2)\alpha(D)\omega^\Gamma} - \frac{4}{5}\ln\left(\frac{2eU}{\hbar\omega^\Gamma}\right)\right. \\ \left. \quad + \frac{1}{5}\ln\left(\frac{\hbar\omega^\Gamma}{\pi eU}\frac{L}{l_{\rm sc}}\right)\right] \quad \text{for} \quad \overline{n} \ll \frac{eU}{\hbar\omega^\Gamma} \ll \frac{L}{\pi l_{\rm sc}}. \end{cases} \quad (40)$$

We show on the right hand side in Fig. 8 the function F_2. Due to the the maximum of $C(x)$ at $x = 1/2$ with $C(1/2) = -\ln(2)$ we obtain that $F_2(x)$ is singular at $x = -\ln 2$. This singularity leads to a sharp edge of the Raman spectrum at the corresponding frequency according to (40).

By taking into account also the broadening of the phonon modes due to the phonon-phonon scattering we obtain that the signal of the actual Raman mode is a convolution of $I_{\rm ep}(\omega)$ (40) with a Lorentzian which has a negative frequency shift and broadening corresponding to the phonon-phonon interaction contribution to the phonon self-energy.

C. Discussion

Next we compare our findings with recent experiments. In Refs. 9, 21 the optical phonon lifetimes and frequency shifts are measured for *suspended* metallic carbon nanotubes at high bias voltage using Raman spectroscopy.

These investigations did not find a response of the G_- and G_+ modes corresponding to the longitudinal and transversal optical $\mathbf{\Gamma}$ modes for all measured nanotubes where only the former mode couples to the electron system at high bias. In fact, it is not well understood which mode response to the bias for a certain nanotube. The nanotube phonon temperature was then measured by two different methods either by the Stokes/anti-Stokes intensity ratio being a function of the phonon Boltzmann factor of the corresponding mode or by mode softening where one compares the softened mode with the known temperature softening which is caused by phonon-phonon scattering. Astonishing, that both methods find phonon temperatures which are in good accordance. They did not provide any hint for a different behavior which we found theoretically above.

Such a different behavior was in fact seen by Oron-Carl *et al.* [6] for metallic nanotubes on a SiO$_2$ *substrate*. They found a mode hardening and a reduction of the linewidth at high bias voltage in comparison to the zero bias voltage values. A real quantitative comparison of our results with the experimental finding is difficult here since the overall broadening and hardening is the additive effect of phonon-phonon scattering leading to softening and broadening of the mode and the hardening effect and a linewidth reduction due to the electron-phonon coupling. That this non-thermal effect was not seen in free-standing nanotubes could be explained by the fact that the heating of many of the crystal modes are much easier for phonons in a suspended crystal in comparison to phonons on a substrate since these phonons could travel especially in long nanotubes substantially until they diffuse out of the system. This is the reason for the experimental finding that large nanotubes show a bias response for the G_+ mode and the G_- mode in general [21]. During this travelling the electron-scattered optical phonons are then thermalized by scattering with acoustic phonons. A true understanding of the different behavior of the frequency shift and broadening between suspended nanotubes and nanotubes on a substrate requires a new theory for suspended nanotubes being out of the scope of this work.

VI. SUMMARY

In this paper we have used the coupled Boltzmann equations for electrons and optical phonons to calculate the current-voltage characteristic of carbon nanotubes lying on a substrate under high bias voltage. First we have studied the coupled electron-phonon Boltzmann system. By taking into account the electron-phonon relaxation time of Ref. 10 which agrees well with experiments, we have determined by numerical fitting the relaxation times of the optical phonons in the single-mode relaxation time approximation. These are much longer for short nanotubes below 1μm than for large ones. The result was obtained by fitting our numerically determined current-
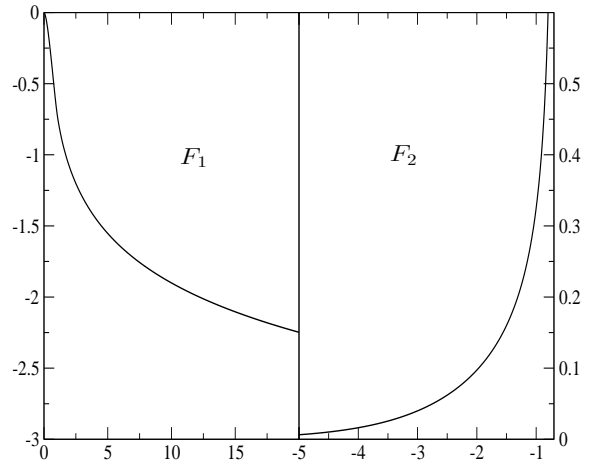

FIG. 8: (Color online) The left panel shows the function $F_1(x)$ (38). On the right hand side we show the Raman lineshape function $F_2(x)$ defined in (39).

voltage curves with the experiments. For short nanotubes, this time did not agree with experimental findings. In Sect III we went beyond the single time relaxation approximation by taking into account also lower lying secondary phonons in the Boltzmann equation which leads us to the conclusion that the phonon relaxation shows a bottleneck in the sector of acoustic phonons for short nanotubes, but not for long nanotubes. We have explained this by the fact that due to the phonon velocity of the lower-lying acoustic phonons, these phonons are redistributed in such a way that at least locally a bottleneck is created for short nanotubes. This leads to a plug in the relaxation path of the optical phonons.

In Section IV, we have considered an analytical solution of the Boltzmann system where we first linearize the electronic equations and use further the assumption of a constant phonon distribution function to solve them in the electronic sector. We have compared our results for the current-voltage characteristic and the phonon distribution function with the numerical findings of Sect. II, Sect. III and the experimental results. We find an especially good agreement in the high-voltage, small length regime. Our analytical theory provides us with the electron and phonon distribution functions as a function of position and momentum. This opens the possibility to calculate the optical phonon broadening and frequency shift due to the coupling of the phonon system to the bias driven electronic system. For zero bias this coupling is the dominant contribution for both quantities

We have then calculated in Sect. V in a charge-current conserved way the broadening and frequency shift of the zone-center optical phonons. We find that the phonon-level broadening, determined at zero bias voltage mainly by the electron-phonon coupling, vanishes at large voltage. The vanishing was explained by a smoothing of

the electron distribution function over the Fermi-level at non-zero bias voltage. For very large voltages and small nanotubes, we found a positive frequency shift. Note that this behavior of a vanishing broadening and positive frequency shift is in contrast to the self-energy contribution of the phonon-phonon interaction to the lower lying hot acoustic phonons. This contribution to the self-energy led to a negative frequency shift and an additional broadening at higher bias due to a temperature increase of the lower lying acoustic phonons.

It was in fact just recently found experimentally by Raman-scattering, that the level broadening decreases and the frequency shift increases for the zone-center optical phonons [6] for increasing bias voltage. In contrast to the very high voltage regime, we found a negative frequency shift at moderate bias voltage and large nanotubes.

Appendix A: Analytic calculation of the current-voltage characteristic

In the following, we carry out the calculation of the current-voltage characteristic and the electron-phonon distribution functions for $eU \gg \hbar\omega$ explicitly by using (1)-(7). To solve the system of equations we use the approximations (18) and (19).

1. Current-voltage characteristic

In the following calculation we go in Fourier-space $f_{L/R}(k_{L/R}, x) = 1/(2\pi)^2 \int dk dt \hat{\hat{f}}_{L/R}(t,k) \exp[i(-kx \mp tv_F \hbar k_{L/R})]$ and use further the function $\hat{f}_{L/R}$ defined by $f_{L/R}(k_{L/R}, x) = 1/(2\pi) \int dt \hat{f}_{L/R}(t,x) \exp[\mp i(tv_F \hbar k_{L/R})]$. With the help of

$$st = \sqrt{1 - \left[\frac{2\overline{n}\cos(\omega t) + \exp(-i\omega t)}{2\overline{n} + 1}\right]^2} \qquad (A1)$$

we obtain from (1)

$$\hat{f}_L = \frac{\hat{n}_F(t)}{De}\left\{e^{-ieE(x-L)\,t/\hbar}\left[st\cosh\left(\frac{|x|}{l^r_{sc}}st\right) + \right.\right.$$
$$\left.\sinh\left(\frac{|x|}{l^r_{sc}}st\right)\right] + e^{-ieEx\,t/\hbar}(1-st^2)^{1/2}\sinh\left(\frac{|x-L|}{l^r_{sc}}st\right)\right\},$$
$$(A2)$$

with

$$De = st\cosh\left(\frac{L}{l^r_{sc}}st\right) + \sinh\left(\frac{L}{l^r_{sc}}st\right), \qquad (A3)$$

where $\hat{n}_F(t)$ is the Fourier-transform of the Fermi-function, i.e. $\hat{n}_F(t) = \int d\epsilon n_F(\epsilon)\exp[-it\epsilon] = +i/(t+i\delta)$. The function f_R is given by (A2) and (A3) with the substitution

$$f_R = f_L[x \to x - L, x - L \to x]. \qquad (A4)$$

We note that one has to take into account during this substitution the absolute value signs in the cosine hyperbolic and sinus hyperbolic arguments in (A2).

In the following, we evaluate (A2) by the help of a residuum integration. With

$$f_L = f_L^{t=0} + f_L^{t\neq 0} \qquad (A5)$$

we obtain for the electron distribution function $f_L^{t=0}$ due to the residuum at $t=0$

$$f_L^{t=0} = [1 - n_F(\epsilon - eE(x-L))]$$
$$+ [n_F(\epsilon - eEx) - n_F(\epsilon - eE(x-L))]\frac{|x-L|}{l^r_{sc}}\frac{1}{1+\frac{L}{l^r_{sc}}}. \qquad (A6)$$

$f_R^{t=0}$ is given by (A6) with the substitution (A4). The $t \neq 0$ singularities are given by the zeros of De. For $L/l^r_{sc} \gg 1$ we obtain for these zeroes

$$st \approx i\frac{\pi n}{\left(1+\frac{L}{l^r_{sc}}\right)} \qquad \text{for} \qquad |st| \lesssim 1, \qquad (A7)$$

$$st \approx i\left(\pi n - \frac{\pi}{2}\right)\frac{l^r_{sc}}{L} \qquad \text{for} \qquad |st| \gtrsim 1. \qquad (A8)$$

With the help of

$$A_1(x_1, x_2) = \frac{1}{2\pi i}\left\{ [1 - n_F(\epsilon - eEx_1)] \right.$$

$$\left. - n_F(\epsilon - eEx_1)\exp\left(-\frac{1}{\overline{n}}\frac{1}{\omega}|\epsilon - eEx_1|\right)\right\}$$

$$\times\sum_{\pm}\pm\ln\left\{1 + \exp\left[-\frac{\pi}{\left(1 + \frac{L}{l_{\mathrm{sc}}^r}\right)}\left(\frac{|\epsilon - eEx_1|}{\omega} \pm i\frac{|x_2|}{l_{\mathrm{sc}}^r}\right)\right]\right\},$$
(A9)

$$A_2(x_1, x_2) = \frac{1}{2\left(1 + \frac{L}{l_{\mathrm{sc}}^r}\right)}\left\{ (1 - n_F(\epsilon - eEx_1)) \right.$$

$$\left. - n_F(\epsilon - eEx_1)\exp\left(-\frac{1}{\overline{n}}\frac{1}{\omega}|\epsilon - eEx_1|\right)\right\}$$

$$\times\sum_{\pm}\left\{1 + \exp\left[\frac{\pi}{\left(1 + \frac{L}{l_{\mathrm{sc}}^r}\right)}\left(\frac{|\epsilon - eEx_1|}{\omega} \pm i\frac{|x_2|}{l_{\mathrm{sc}}^r}\right)\right]\right\}^{-1}$$
(A10)

we obtain for $f^{t\neq 0}$ due to the singularities in the regime $|st| \lesssim 1$ (A7)

$$f_L^{t\neq 0} = A_1(x, x-L) + A_1(x-L, x) + A_2(x-L, x). \quad (A11)$$

$f_R^{t\neq 0}$ is given by $f_L^{t\neq 0}$ with the substitution (A4).

Finally, we have to discuss the contribution of singularities $|st| \gtrsim 1$ (A8) to $f^{t\neq 0}$. Due to the Fourier-exponent, these terms are exponentially suppressed beyond a small energy strip of range $|\Delta\epsilon|/\omega \gtrsim 1$ in comparison to terms calculated with residua $|st| \lesssim 1$. From the discussion above and the following discussions we obtain that these terms are not relevant in the range $eU/\hbar\omega \gg 1$, $L \gg l_{\mathrm{sc}}^r$ for the determination of the phonon distribution function. We also note without an explicit calculation here but which can be shown with similar methods as for the current calculation of the $|st| \lesssim 1$ singularities below that the current from the $|st| \gtrsim 1$ singularities is negligible in comparison to the current calculated from the singularities $|st| \lesssim 1$. This current contribution will be calculated explicitly in the following.

The current I can be calculated by the help of $I = (4e/h)\int d\epsilon(f_R - f_L)$. This is best done by carrying out the integration at the boundaries $x = 0$ or $x = L$ of the nanotube. From (A6) and (A11) and the corresponding expressions for f_R, we obtain the following current-voltage characteristic

$$I = 4\frac{e}{h}\left[\hbar\omega B_1\left(\frac{1 + \frac{L}{l_{\mathrm{sc}}^r}}{\pi\overline{n}}\right) + e\frac{U}{\left(1 + \frac{L}{l_{\mathrm{sc}}^r}\right)}\right] \quad (A12)$$

with

$$B_1(x) = \frac{1}{2\pi}\left[H\left(\frac{x}{2} - 1\right) - H\left(\frac{x}{2}\right) + \ln(4) + 2H(x)\right]$$
(A13)

where $H(x) = \gamma + \Psi(x+1)$ and γ is the Euler-Mascheroni constant, $\Psi(x)$ is the digamma function. We show in Fig. 6 the function $B_1(x)$.

2. Phonon distribution function

Next we calculate the phonon distribution function $\overline{n}(x)$ (15). We carry out this calculation only in the leading order in l_{sc}^r/L. In order to simplify our notation we define $\tilde{x} \equiv x/L$. Next we calculate from (A6), (A11) and the corresponding equation for f_R (A4) the phonon distribution function in the regime $\pi eU \gg \hbar\omega L/l_{\mathrm{sc}}$

a. Phonon distribution function for $\pi eU \gg \hbar\omega L/l_{\mathrm{sc}}$

In the following, we only have to determine the $k > 0$ phonons since we find from symmetry arguments that

$$n(k, x) = n(-k, -x). \quad (A14)$$

To simplify our notation we define the following regimes for $k > 0$

$$\mathcal{R}_1 : \tilde{x} < \frac{1}{2}, eU(1 - \tilde{x}) > \frac{v_F\hbar k}{2} > eU\tilde{x}, \quad (A15)$$

$$\mathcal{R}_2 : \tilde{x} > \frac{1}{2}, eU\tilde{x} > \frac{v_F\hbar k}{2} > eU(1 - \tilde{x}),$$

$$\mathcal{R}_3 : \tilde{x} < \frac{1}{2}, eU\tilde{x} > \frac{v_F\hbar k}{2} \text{ or } \tilde{x} > \frac{1}{2}, eU(1 - \tilde{x}) > \frac{v_F\hbar k}{2}.$$

We obtain for the phonon-Boltzmann equation (4) by using (A6), (A11) and (A4)

$$\frac{\partial}{\partial x}n(k, x) = K_1 n(k, x) + K_2 \quad (A16)$$

with

$$\mathcal{R}_1 : K_1 = -\frac{1}{v_{\mathrm{ph}}}\left(\frac{s^p}{\tau_{\mathrm{ep}}}\frac{l_{\mathrm{sc}}}{L} + \frac{1}{\tau_{\mathrm{op}}}\right), K_2 = \frac{s^p\tilde{x}}{v_{\mathrm{ph}}\tau_{\mathrm{ep}}},$$

$$\mathcal{R}_2 : K_1 = -\frac{1}{v_{\mathrm{ph}}}\left(-\frac{s^p}{\tau_{\mathrm{ep}}}\frac{l_{\mathrm{sc}}}{L} + \frac{1}{\tau_{\mathrm{op}}}\right), K_2 = \frac{s^p(1 - \tilde{x})}{v_{\mathrm{ph}}\tau_{\mathrm{ep}}},$$

$$\mathcal{R}_3 : K_1 = -\frac{1}{v_{\mathrm{ph}}\tau_{\mathrm{op}}}, K_2 = 2\frac{s^p\tilde{x}(1 - \tilde{x})}{v_{\mathrm{ph}}\tau_{\mathrm{ep}}}. \quad (A17)$$

By taking into account the boundary conditions $n(k, 0) = 0$ and further $v_{\mathrm{ph}}\tau_{\mathrm{op}} \ll L$ we obtain for $n(k, x)$ in $\mathcal{R}_1$ and $\mathcal{R}_3$

$$\mathcal{R}_1 : n_{\mathcal{R}_1}(k, x) = -\frac{s^p L}{v_{\mathrm{ph}}\tau_{\mathrm{ep}}}\frac{1}{K_1 L}\tilde{x}, \quad (A18)$$

$$\mathcal{R}_3 : n_{\mathcal{R}_3}(k, x) = -\frac{s^p L}{v_{\mathrm{ph}}\tau_{\mathrm{ep}}}\frac{1}{K_1 L}2\tilde{x}(1 - \tilde{x}). \quad (A19)$$

We point out here that according to (A17) the expressions for K_1 in (A18) and (A19) are different in the different regimes (A15). We obtain in these regions the

same solutions $n(k,x)$ of (2) as we would set immediately $v_{\mathrm{ph}} = 0$ from the beginning. This is not true for $n(k,x)$ in $\mathcal{R}_2$. We obtain especially in the regions where $l_{\mathrm{sc}}/L \sim \tau_{\mathrm{ep}}/\tau_{\mathrm{op}}$ that the neglection of the v_{ph} term in (2) is not allowed. Such parameter values lead to the result that the phonon distribution function at the boundary of the nanotube increases which is in fact seen in Fig. 5. In the regime $\mathcal{R}_2$ we obtain from (A16), (A17)

$$\mathcal{R}_2 : n_{\mathcal{R}_2}(k,x) = n_0(k,x_0(k))e^{K_1(x-x_0(k))} + \frac{s^p L}{v_{\mathrm{ph}}\tau_{\mathrm{ep}}}\frac{1}{K_1 L}$$
$$\times \left[\frac{1}{K_1 L}(1+K_1 x) - e^{K_1(x-x_0(k))}\frac{1}{K_1 L}(1+K_1 x_0(k)) \right] \tag{A20}$$

where $x_0(k) = L(1/2 + |1/2 - v_F \hbar k/2eU|)$, $n_0(k,x_0(k)) = n_{\mathcal{R}_3}(k,x_0(k))$ for $v_F \hbar k/2 < eU/2$ and $n_0(k,x_0(k)) = 0$ for $v_F \hbar k/2 > eU/2$.

We now use the abbreviation

$$\tilde{K}_1 = K_1 L. \tag{A21}$$

Next, we calculate the phonon density $\overline{n}(x)$ (15). According to the discussion above, we obtain

$$\overline{n}(x) \approx (\overline{n}_{\mathcal{R}_1}(L-x) + \overline{n}_{\mathcal{R}_2}(x))\theta(\tilde{x}-1/2) \tag{A22}$$
$$+ (\overline{n}_{\mathcal{R}_1}(x) + \overline{n}_{\mathcal{R}_2}(L-x))\theta(1-(\tilde{x}-1/2)) + 2\overline{n}_{\mathcal{R}_3}(x)$$

where $\overline{n}_{\mathcal{R}_i}$ are the energy averaged phonon distribution functions (A18), (A19) and (A20) according to (15) where the integration region are restricted to $\mathcal{R}_i$ (A15). These are given by

$$\overline{n}_{\mathcal{R}_1}(x) = -\frac{1}{2}\frac{s^p L}{v_{\mathrm{ph}}\tau_{\mathrm{ep}}}\frac{1}{\tilde{K}_1}\tilde{x}(1-2\tilde{x}), \tag{A23}$$

$$\overline{n}_{\mathcal{R}_3}(x) = -\frac{s^p L}{v_{\mathrm{ph}}\tau_{\mathrm{ep}}}\frac{1}{\tilde{K}_1}\left(\frac{1}{2}-\left|\tilde{x}-\frac{1}{2}\right|\right)\tilde{x}(1-\tilde{x}) \tag{A24}$$

and

$$\overline{n}_{\mathcal{R}_2}(x) \approx \frac{s^p L}{v_{\mathrm{ph}}\tau_{\mathrm{ep}}}\frac{1}{\tilde{K}_1}\left\{\left(\tilde{x}-\frac{1}{2}\right)(\tilde{x}-1)\right. \tag{A25}$$
$$\left. + \frac{1}{\tilde{K}_1}\left[\left(2\tilde{x}-\frac{3}{2}\right)+\frac{1}{2}e^{\tilde{K}_1(\tilde{x}-\frac{1}{2})}\right]+\frac{2}{\tilde{K}_1^2}\left(1-e^{\tilde{K}_1(\tilde{x}-\frac{1}{2})}\right)\right\}$$

where we took into account that $L/v_{\mathrm{ph}}\tau_{\mathrm{op}} \gg 1$. Finally, we calculate the position averaged phonon distribution function $\overline{n} = \int dx\,\overline{n}(x)/L$. We obtain

$$\overline{n} \approx 2(\overline{n}_{\mathcal{R}_1} + \overline{n}_{\mathcal{R}_2} + \overline{n}_{\mathcal{R}_3}) \tag{A26}$$

with

$$\overline{n}_{\mathcal{R}_1} \approx -\frac{s^p L}{v_{\mathrm{ph}}\tau_{\mathrm{ep}}}\frac{1}{\tilde{K}_1}\frac{1}{48}, \tag{A27}$$

$$\overline{n}_{\mathcal{R}_3} \approx -\frac{s^p L}{v_{\mathrm{ph}}\tau_{\mathrm{ep}}}\frac{1}{\tilde{K}_1}\frac{13}{192} \tag{A28}$$

and

$$\overline{n}_{\mathcal{R}_2} \approx \frac{s^p L}{v_{\mathrm{ph}}\tau_{\mathrm{ep}}}\frac{1}{\tilde{K}_1}\left[-\frac{1}{48}+\frac{1}{\tilde{K}_1^2}\right.$$
$$\left. +\left(\frac{1}{2\tilde{K}_1^2}-\frac{2}{\tilde{K}_1^3}\right)\left(e^{\tilde{K}_1/2}-1\right)\right]. \tag{A29}$$

By taking into account the definition of $\tilde{K}_1$ (A21), (A17) we obtain that (A26) is the relation which determines the energy-position averaged phonon distribution function $\overline{n}$ (18).

Let us first assume that $\tilde{K}_1 \gg 1$ in region $\mathcal{R}_2$. From expression (A29) we find that there is no solution in this parameter region for (A26) since $L/v_{\mathrm{ph}}\tau_{\mathrm{ep}} \gg 1$ and $v_F\tau_{\mathrm{ep}} = 130$nm.

Next we assume that $\tilde{K}_1 \ll -1$ in the region $\mathcal{R}_2$. From (A17) we find then that $\tilde{K}_1 \approx -L/v_{\mathrm{ph}}\tau_{\mathrm{op}}$ in the regions $\mathcal{R}_i$. By using (A26) we obtain

$$\overline{n} \approx \frac{13}{96}\frac{s^p\tau_{\mathrm{op}}}{\tau_{\mathrm{ep}}} \quad \text{for} \quad L \gg \frac{v_{\mathrm{ph}}\tau_{\mathrm{ep}}}{\frac{26s^p\tau_{\mathrm{op}}}{96\tau_{\mathrm{ep}}}+1}\left(\frac{s^p\tau_{\mathrm{op}}}{\tau_{\mathrm{ep}}}-1\right). \tag{A30}$$

For $\tau_{\mathrm{op}} = 9.1$ps we obtain $\overline{n} = 5.3$. This leads to $l_{\mathrm{sc}} = 11.1$nm. This value is in excellent agreement with the experimentally determined value $l_{\mathrm{sc}} \approx 10-11$nm [3, 4]. From (A22), (A23), (A24) and (A25) we obtain that the phonon distribution function $\overline{n}(x)$ is zero at the boundary of the nanotube. By using the scattering parameters in (14) we further obtain the validity of (A30) for $L \gg 426$nm.

For smaller nanotube lengths one has $\tilde{K}_1 \sim 0$. By explicit calculation we obtain for $L/v_{\mathrm{ph}}\tau_{\mathrm{op}} \gg 1$ and $\tilde{K}_1 \sim 0$ that $\overline{n}_{\mathcal{R}_1}, \overline{n}_{\mathcal{R}_3} \ll \overline{n}_{\mathcal{R}_2}$. By taking only $\overline{n}_{\mathcal{R}_2}$ into account in (A22) and (A26) we obtain for the energy averaged phonon distribution function by Taylor expanding (A25) with respect to $\tilde{K}_1$

$$\overline{n}(x) \approx \frac{s^p L}{v_{\mathrm{ph}}\tau_{\mathrm{ep}}}\left(\frac{1}{4}|\tilde{x}-1/2|^2-\frac{1}{3}|\tilde{x}-1/2|^3\right) \tag{A31}$$

and for (A26) with (A29)

$$\overline{n} \approx \frac{s^p L}{v_{\mathrm{ph}}\tau_{\mathrm{ep}}}\frac{1}{96}. \tag{A32}$$

From (A31) we get an increasing behavior of the phonon distribution function at the boundary of the nanotube in agreement with Fig. 5.

Finally, we calculate the phonon distribution function $\overline{n}$ by solving (A26) for $\overline{n}$ with (A27), (A28) and (A29) numerically as a function of the nanotube length L. The result is shown in Fig. 7. We obtain that the decrease of $\overline{n}$ for in the direction of small L given by (A32) is not very large such that we can assume approximately the validity of (A30) in the whole regime $L \gtrsim 50$nm. Next, we calculate the phonon distribution function for $\pi eU \ll \hbar\omega L/l_{\mathrm{sc}}$.

b. Phonon distribution function for $\pi eU \ll \hbar\omega L/l_{sc}$

By taking into account (A6), (A11) and (A4) we obtain that $n(k,x) \neq n_B^{ac}$ only in the regime $|\pi(v_F|k|/2\omega)l_{sc}/L| \lesssim 1$ where we use that $\overline{n} \lesssim 1$ as will be shown below. In this regime we obtain for $k > 0$ (A16) with

$$K_1 = -\frac{1}{v_{ph}}\left[\frac{s^p}{\tau_{ep}}\frac{l_{sc}}{L}\left(\frac{\cos(\pi\tilde{x})}{1-\cos^2(\pi\tilde{x})}\right) + \frac{1}{\tau_{op}}\right],$$
$$K_2 = \frac{s^p}{4v_{ph}\tau_{ep}} \tag{A33}$$

where again (A14) holds. We now assume that $l_{sc}/L \ll \tau_{ep}/\tau_{op}$ which is good fulfilled in the large length regime

where we have (14) $\tau_{ep}/\tau_{op} \approx 0.22$. Then we obtain for $|\pi(v_F|k|/2\omega)l_{sc}/L| \lesssim 1$

$$n(k,x) \approx \frac{s^p}{4}\frac{\tau_{op}}{\tau_{ep}}. \tag{A34}$$

We point out that (A34) is not valid in the small regime where $0 \leq |\epsilon| \leq eU, \overline{n}\omega$. We obtain a position dependent numerical prefactor to (A34) in this regime. From (A34) we are able to calculate $\overline{n}(x)$ and $\overline{n}$ given by

$$\overline{n}(x) = \overline{n} \approx \frac{s^p}{4}\frac{\tau_{op}}{\tau_{ep}}. \tag{A35}$$

[1] Z. Yao, C. L. Kane, and C. Dekker, Phys. Rev. Lett. **84**, 2941 (2000).
[2] V. Perebeinos, J. Tersoff, and P. Avouris, Phys. Rev. Lett. **94**, 086802 (2005).
[3] J. Y. Park, S. Rosenblatt, Y. Yaish, V. Sazonova, H. stnel, S. Braig, T. A. Arias, P. W. Brouwer, and P. L. McEuen, Nano Letters **4**, 517 (2004).
[4] A. Javey, J. Guo, M. Paulsson, Q. Wang, D. Mann, M. Lundstrom, and H. Dai, Phys. Rev. Lett. **92**, 106804 (2004).
[5] E. Pop, D. A. Mann, K. E. Goodson, and H. Dai, J. Appl. Phys. **101**, 093710 (2007).
[6] M. Oron-Carl and R. Krupke, Phys. Rev. Lett. **100**, 127401 (2008).
[7] M. Steiner, M. Freitag, V. Perebeinos, J. C. Tsang, J. P. Small, M. Kinsoshita, D. Yuang, J. Liu, and P. Avouris, Nature Nanotech. **4**, 320 (2009).
[8] P. Sundqvist, F. J. Garcia-Vidal, F. Flores, M. Moreno-Moreno, C. Gómez-Navarro, J. S. Bunch, and J. Gómez-Herrero, Nano Lett. **7**, 2568 (2007).
[9] A. W. Bushmaker, V. V. Deshpande, M. W. Bockrath, and S. B. Cronrin, Nano Lett. **7**, 3618 (2007).
[10] M. Lazzeri, S. Piscanec, F. Mauri, A. C. Ferrari, and J. Robertson, Phys. Rev. Lett. **95**, 236802 (2005).
[11] M. Lazzeri and F. Mauri, Phys. Rev. B **73**, 165419 (2006).
[12] C. Auer, F. Schürrer and C. Ertler, Phys. Rev. B **74**, 165409 (2006); C. Auer, F. Schürrer and C. Ertler, J. Comput. Electron **6**, 325 (2007).
[13] P. A. Sundqvist, F. J. Garcia-Vidal, and F. Flores, Phys. Rev. B **78**, 205427 (2008).
[14] M. A. Kuroda, A. Cangellaris, and J.-P. Leburton, Phys. Rev. Lett. **95**, 266803 (2005).
[15] M. A. Kuroda and J.-P. Leburton, Phys. Rev. B **80**, 165417 (2009).
[16] See, e.g., G. P. Srivastava, *The Physics of Phonons*, (Hilger, Bristo, 1990).
[17] S. Piscanec, M. Lazzeri, F. Mauri, A. C. Ferrari, and J. Robertson, Phys. Rev. Lett. **93**, 185503 (2004).
[18] D. Song, F. Wang, G. Dukovic, M. Zheng, E. D. Semke, L. E. Brus, and T. F. Heinz, Phys. Rev. Lett. **100**, 225503 (2008).
[19] K. Kang, T. Ozel, D. G. Cahill, and M. Shim, Nano Lett.

8, 4642 (2008).
[20] R. Rao, J. Menendez, C. D. Poweleit, and A. M. Rao, Phys. Rev. Lett. **99**, 047403 (2007). N. Bonini, R. Rao, A. M. Rao, N. Marzari, and J. Menéndez, phys. stat. sol. (b) **245**, 2149 (2008).
[21] V. V. Deshpande, S. Hsieh, A. W. Bushmaker, M. Bockrath, and S. B. Cronin, Phys. Rev. Lett. **102**, 105501 (2009).
[22] S. Datta *Electronic Transport in Mesoscopic Systems*, (Cambridge University Press, Cambridge, 1995).
[23] H. Ishii, S. Roche, N. Kobayashi, and K. Hirose, Phys. Rev. Lett. **104**, 116801 (2010).
[24] G. Pennington, S. J. Kilpatrick, and A. E. Wickenden, Appl. Phys. Lett. **93**, 093110 (2008).
[25] N. Vandecasteele, M. Lazzeri, and F. Mauri, Phys. Rev. Lett. **102**, 196801 (2009).
[26] H. Suzuura and T. Ando, J. Phys. Soc. Jpn. **77**, 044703 (2008).
[27] V. V. Aristov, *Direct methods for solving the Boltzmann equation and study of nonequilibrium flows*, (Kluwer Academic Publishers, Dordrecht, 2001).
[28] We use a space and momentum grid with 500 points. The momentum range is then given by $5eU/(\hbar v_F)$.
[29] K. Ishikawa and T. Ando, J. Phys. Soc. Jpn. **75**, 084713 (2006).
[30] N. Bonini, M. Lazzeri, N. Marzari, and F. Mauri, Phys. Rev. Lett. **99**, 176802 (2007).
[31] S. Jursenas, A. Zukauskas and R. Baltramiejunas, J. Phys.: Condens. Matter **4**(49), 9987 (1992).
[32] S. P. Hepplestone and G. P. Srivastava, Phys. Rev. B **74**, 165420 (2006).
[33] R. Saito, T. Takeya, T. Kimura, G. Dresselhaus, and M S. Dresselhaus, Phys. Rev. B **57**, 4145 (1998).
[34] G. D. Mahan, Phys. Rev. B **65**, 235402 (2002).
[35] S. Zhang, M. Xia, S. Zhao, T. Xu, and E. Zhang, Phys. Rev. B **68**, 075415 (2003).
[36] H. Haug and A. -P. Jauho, *Quantum Kinetics in Transport and Optics of Semiconductors*, (Springer, Heidelberg, 1998).
[37] G. Baym and L. P. Kadanoff, Phys. Rev. **124**, 287 (1961).
[38] M.S. Dresselhaus, G. Dresselhaus, R. Saito and A. Jorio, Phys Report **409**, 47 (2005).